ELSEVIER

Journal of Power Sources 58 (1996) 23–28

JOURNAL OF POWER SOURCES

Effect of cobalt addition to nickel hydroxide as a positive material for rechargeable alkaline batteries

Ken-ichi Watanabe [a], Mitsuru Koseki [a], Naoaki Kumagai [b]

[a] *Shin-Kobe Electric Machinery Co., Ltd., Shinjyuku-Mitsui Building, No. 1-1, 2-chome, Nishishinjyuku, Shinjyuku-Ku, Tokyo 163, Japan*

[b] *Department of Applied Chemistry and Molecular Science, Faculty of Engineering, Iwate University, Morioka 020, Japan*

Received 25 August 1995; accepted 31 October 1995

Abstract

Nickel hydroxide powder is used widely as an active material in pasted-type nickel electrodes. The effect on the electrochemical behaviour of cobalt addition (0.19–9.9 wt.%) to the nickel hydroxide powder is investigated. The physical properties of several nickel hydroxide powders containing different amounts of cobalt compound are examined by inductively coupled spectroscopy, laser diffraction, BET, X-ray diffraction and scanning electron microscopy measurements. The interlayer distance of the layered nickel hydroxide diminishes to a small value with increase in cobalt content. Moreover, the charge and discharge potentials of nickel hydroxide samples decrease with an increase in cobalt content. The chemical diffusion coefficients of the proton($\tilde{D}$) in the nickel hydroxide samples with different amounts of cobalt are measured by a current-pulse relaxation technique. The $\tilde{D}$ and D_0 values increase with an increase in cobalt content, and the activation energy for proton diffusion is in the 0.20–0.33 eV range.

Keywords: Rechargeable alkaline batteries; Nickel hydroxide; Cobalt; Positive materials

1. Introduction

In recent years, much interest has focused on the development of rechargeable alkaline batteries with high energy densities. In order to improve energy density, pasted-type nickel electrodes have been developed [1,2]. This type of nickel electrode uses nickel hydroxide ($Ni(OH)_2$) as the active material in a nickel foam substrate.

The addition of cobalt to the positive electrodes of rechargeable alkaline batteries has been studied extensively [2–11]. These reports present some conflicting results, probably due to differences in: the crystallite size of the nickel hydroxide [12]; the electrode types (such as the impregnation type and pasted type); the kind of electrolytes used in the experiments (such as KOH, NaOH and LiOH), and the cells.

In the present work, several kinds of nickel hydroxide powder samples with different cobalt contents have been used as positive electrodes in rechargeable alkaline batteries. The electrochemical properties, including charge/discharge characteristics of the nickel hydroxide powders, are investigated as a function of cobalt content. Furthermore, the kinetics of proton insertion into the crystal lattice of nickel hydroxide are studied using a current-pulse relaxation technique.

2. Experimental

2.1. Preparation of electrode materials

Nickel foam (2 cm×2 cm, Sumitomo Electric Industries Ltd.) was used as the nickel electrode substrate. The following five kinds of β-type nickel hydroxide (β-$Ni(OH)_2$) powders (A–E) were used as positive materials: samples A and C from Nihon Kagaku Sangyo Company; samples B, D and E from Tanaka Chemical Corporation. These nickel hydroxide samples with different cobalt contents were obtained by adding an alkaline solution to the mixed Ni^{2+} and Co^{2+} solutions with different Co^{2+} contents.

Cobalt metal powder (obtained from N.V. Union Miniere S.A.) was added at 5 wt.% to the hydroxide powders to increase and stabilize the utilization of the active materials [1,2]. Hydroxypropylmethyl cellulose (HPMC) (Shin-Etsu Chemical Co.) and polytetrafluoroethylene (PTFE) dispersion (Daikin Industries Ltd.) were used as binders.

2.2. Analysis of nickel hydroxide samples

The chemical composition of each of the nickel hydroxide powder samples was determined with an inductively coupled argon plasma emission spectrophotometer (Model P-5200,

SSDI 0378-7753(95)02272-3

Hitachi Ltd.). The surface area was evaluated by the BET adsorption method using a surface area analyser (Model MIC-2205, Micromeritics Ltd.). The particle size distribution of the hydroxide powder samples was obtained from laser diffraction measurements (Model SPA, Microtrack Ltd.). Scanning electron microscopic (SEM) observations were performed with an S-900 microscope (Hitachi Ltd.). X-ray diffraction measurements were conducted with a RINT-1100 diffractometer (Rigaku Ltd.), Cu Kα radiation with nickel filter at 40 kV and 20 mA.

2.3. Preparation of nickel electrode

The preparation of the nickel electrode has been described in Ref. [12]. The geometrical surface area of the nickel electrode was 4 cm^2 and the weight of nickel hydroxide in the powders (A–E) was ~0.14 g cm^{-2}. The nickel electrodes were spot welded with a 6 mm nickel ribbon as a current collector.

2.4. Electrochemical measurement of nickel electrode

Charge/discharge curves were obtained for a glass beaker cell. A nickel mesh was used as the counter electrode, 30 wt.% KOH as the electrolyte, and Hg/HgO (30 wt.% KOH) as the reference electrode. The electrolysis cell was placed in an incubator held at a given temperature (±2 °C). Charging was performed initially at a rate of 7.0 mA cm^{-2} for 6 h. The charging capacity was about 120% of the theoretical capacity of the positive electrode. Discharging was then carried out at a rate of 7.0 mA cm^{-2} down to 0.1 V versus Hg/HgO at 20 °C. Charge/discharge cycles were performed at a given temperature (20 or 40 °C) with the same charge/discharge rate of 7.0 mA cm^{-2}.

The theoretical capacity of nickel hydroxide is 289 mAh per g of active material by assuming the electrode reaction to be:

$$Ni(OH)_2 + OH^- \rightleftarrows NiOOH + H_2O + e^- \quad (1)$$

The composition of the working electrode was changed by coulombmetric titration. To reach equilibrium after coulombmetric titration required a period of 20 to 50 h at a constant temperature in order to obtain uniform H^+-ion distribution throughout the working electrode. Equilibrium was considered to have been reached when the open-circuit voltage (OCV) was stabilized to less than 0.1 mV h^{-1} at a constant temperature.

The chemical proton diffusion coefficients, $\tilde{D}$, in the hydroxides were measured by the current-pulse relaxation (CPR) technique described by Basu and Worrell [13], Kumagai et al. [14] and Dickens et al. [15] using the following formula for the time dependence of the transient voltage (ΔE):

$$\Delta E = IV_m\tau(dE/dn)/FA(\pi\tilde{D}t)^{1/2} \quad (2)$$

where I is a current pulse (300 mA), V_m the molar volume (22.61 cm^3, which was obtained by assuming the sample to be β-nickel hydroxide), τ is the duration of the pulse (8 s), (dE/dn) the slope of the OCV as a function of capacity, and A the apparent geometric area (4 cm^2), which is assumed to be true in the present work. In Eq. (2), $n = 0$–1 is used by assuming the following electrode reaction:

$$H_nNiOOH \rightleftarrows NiOOH + nH^+ + ne^- \quad (n = 0-1) \quad (3)$$

A current-pulse generator (Model HC-113, Hokuto Denko Ltd.) was used. The resulting potential–time transients were recorded on an oscilloscope for short durations and on a voltage recorder over long periods.

3. Results and discussion

3.1. Physical properties of nickel hydroxide samples

The chemical compositions and physical properties of the nickel hydroxide samples are presented in Table 1. The cadmium contents are nearly zero, but the cobalt contents are different in each sample. The mean diameter of these samples is in the range 11 to 17 μm, and BET surface areas are between 22 and 38 $m^2\ g^{-1}$.

Electron micrographs of the nickel hydroxide samples are given in Fig. 1. At low magnification, the samples appear spherical, but at a higher magnification they are found to consist of many tiny crystals.

All these samples are made up of stacks of small, thin, plate-like crystals. Such a crystal form of nickel hydroxide displayed excellent charge/discharge behaviour and a higher $\tilde{D}$ value, as reported in our earlier work [12].

Table 1
Physical properties of nickel hydroxide samples

Sample	Chemical composition (wt.%)			Mean diameter (μm)	BET surface area ($m^2\ g^{-1}$)
	Ni	Co	Cd		
A	61.9	0.19	<0.01	14	38
B	61.2	0.65	<0.01	17	25
C	59.6	2.1	<0.01	12	27
D	57.0	4.6	<0.01	14	22
E	51.5	9.9	<0.01	11	30

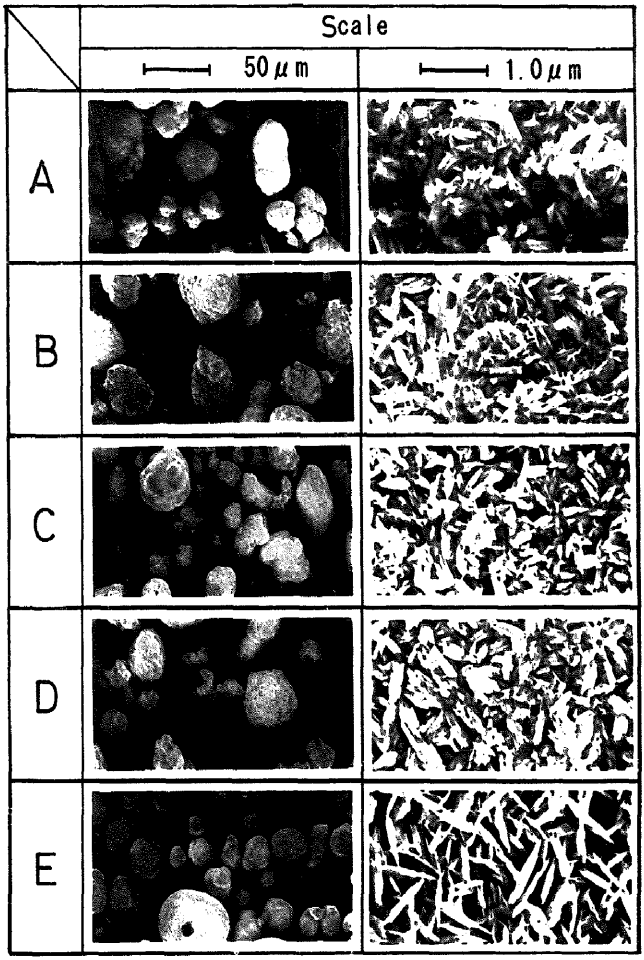

Fig. 1. Electron micrographs of: (A) 0.19 wt.% Co, (B) 0.65 wt.% Co; (C) 2.1 wt.% Co; (D) 4.6 wt.% Co, and (E) 9.9 wt.% Co.

The X-ray diffraction (XRD) patterns of the samples are presented in Fig. 2. These samples have different cobalt contents and give almost the same XRD pattern due to β-type nickel hydroxide (β-$Ni(OH)_2$). This fact shows that the cobalt component is incorporated in the crystal lattice of the β-type nickel hydroxide. The full width of half-maximum intensity (FWHM) and the d values of the respective samples in the (001), (100) and (101) reflections are listed in Table 2. The FWHMs tend to decrease with an increase in the cobalt content.

The samples A–D have almost the same d_{100} and d_{101} values. On the other hand, the d_{001} values (that give the

Table 2
FWHM and d values in (001), (100) and (101) diffraction lines of nickel hydroxide samples

Sample	(001)		(100)		(101)	
	FWHM (deg)	d_{001} (nm)	FWHM (deg)	d_{100} (nm)	FWHM (deg)	d_{101}(nm)
A	1.095	0.4682	0.450	0.2709	1.153	0.2342
B	0.729	0.4677	0.390	0.2709	0.995	0.2342
C	0.935	0.4667	0.411	0.2709	0.931	0.2341
D	0.815	0.4657	0.415	0.2709	0.985	0.2342
E	0.841	0.4633	0.430	0.2703	0.872	0.2336

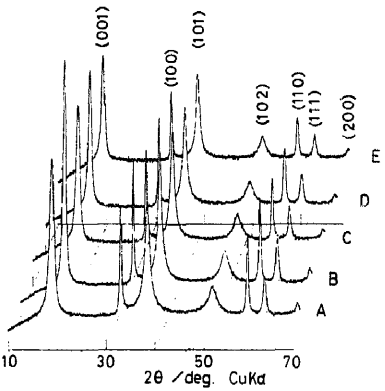

Fig. 2. XRD patterns of samples showing the Miller indices of β-Ni(OH)$_2$ samples: (A) 0.19 wt.% Co; (B) 0.65 wt.% Co; (C) 2.1 wt.% Co; (D) 4.6 wt.% Co, and (E) 9.9 wt.% Co.

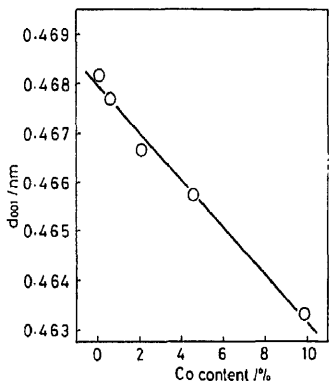

Fig. 3. Effect of cobalt content on d_{001} value.

interlayer distance of a brucite-type structure with a hexagonal unit cell) decrease with increase in the cobalt content, as seen in Fig. 3. This reveals the formation of a solid-solution oxide. The decrease in the d_{001} values is probably caused by the substitution of Ni^{2+} ions with an ionic radius of 0.083 nm [16] with Co^{2+} ions with a smaller ionic radius of 0.079 nm [16].

3.2. Electrochemical characteristics of the nickel hydroxide electrode

Typical charge and discharge curves of several nickel electrodes (samples A, D and E) measured at 20 and 40 °C are shown in Fig. 4. For the charge curves, the charge potential decreases with an increase in the cobalt content in the charge-capacity range from 0 to ~250 mAh per g of Ni(OH)$_2$. On the other hand, in the charge-capacity region above 250 mAh per g of Ni(OH)$_2$, an obvious charge plateau with a higher potential appeared at cobalt contents greater than 4.6 wt.%.

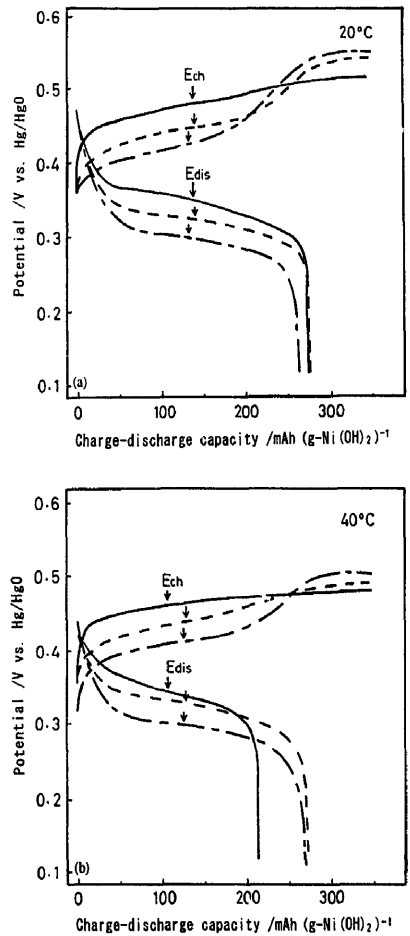

Fig. 4. Charge/discharge curves of samples measured at (a) 20 °C, and (b) 40 °C with a charge/discharge rate of 7.0 mA cm^{-2}. (———) A: 0.19 wt.% Co; (– – –) D: 4.6 wt.% Co, and (– · –) E: 9.9 wt.% Co. E_{ch}: charge potential at half-charged state, and E_{dis}: discharge potential at half-discharged state. Charge/discharge curves were measured on the second cycle.

This higher potential region may be due to the oxidation reaction of the cobalt component, i.e., $Co^{2+} \rightarrow Co^{3+} + e^-$.

The discharge curves also decrease with an increase in the cobalt content. Moreover, as seen in the discharge curves measured at 40 °C, cobalt addition above 4.6 wt.% caused a considerable increase in the capacity.

The charge potential, E_{ch}, obtained at the half-charged state, and the discharge potential, E_{dis}, obtained at the half-discharged state in the charge/discharge curves of Fig. 4, are presented in Fig. 5 as a function of cobalt content. Both the E_{ch} and E_{dis} values decrease with increase in the cobalt content. The intermediate potential between the E_{ch} and E_{dis} values would correspond to the equilibrium electrode potential

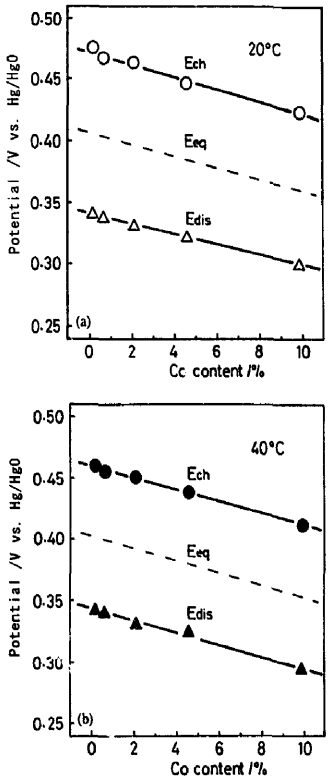

Fig. 5. Variations in E_{ch}, E_{dis} and E_{eq} as a function of cobalt content in the hydroxide.

(E_{eq}) for Eq. (2). Thus, the equilibrium electrode potential is found to decline with increase in cobalt content.

3.3. Proton diffusion behaviour in the nickel hydroxide electrode

Variations in the closed-circuit potential and quasi-equilibrium open-circuit potential are presented in Fig. 6 as a function of discharge capacity for sample D. When the current was interrupted after discharge to various capacities, the potentials of the nickel electrode recovered gradually towards the equilibrium state. This would be caused by a slow diffusion of protons from the surface of the electrode towards the bulk.

The diffusion of protons in nickel oxide was investigated quantitatively using the CPR technique (Eq. (2)). The values of dE/dn in Eq. (2) were obtained from the linear relationships between the OCV and discharge capacity in the range 50–200 mAh per g $Ni(OH)_2$ in Fig. 6. A typical transient voltage (ΔE) in sample D observed after the passage of a current pulse is plotted against $1/\sqrt{t}$ in Fig. 7. The $\Delta E/t$ relationship was found to be linear over the period 32 to 400 s. During the initial period (0 to 32 s), however, the variation

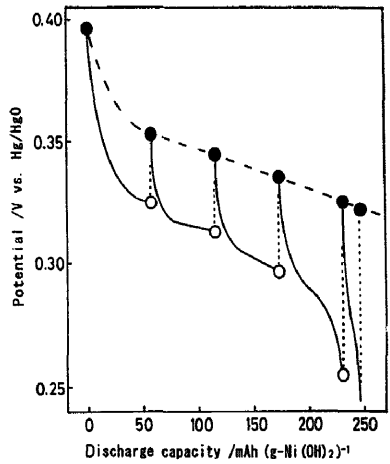

Fig. 6. Closed-circuit and open-circuit potentials as a function of discharge capacity sample D at 20 °C: (●) Open-circuit potential, and (○) closed-circuit potential. Discharge-current density = 7.0 mA cm^{-2}. Both types of potential were measured on the second discharge.

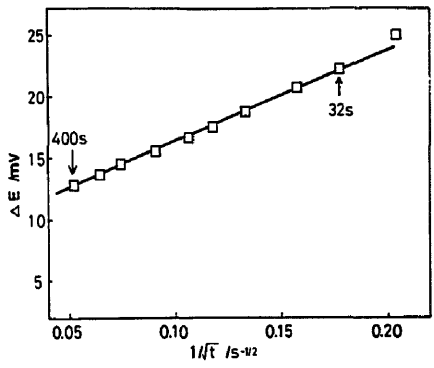

Fig. 7. Typical plot of observed voltage (ΔE) against $1/\sqrt{t}$ for sample D. Amplitude of current pulse = 300 mA, and temperature = 20 °C.

was not linear. This may be attributed to an 'electrolyte effect' caused by the penetration of the electrolyte into the porous electrode [13]. The slope of the linear region was used to calculate the chemical diffusion of protons, $\tilde{D}$, in the nickel oxide.

The temperature dependence of $\tilde{D}$ in each sample is shown in Fig. 8. The $\tilde{D}$ values increase with increase in cobalt content. The value of $\tilde{D}$ cannot be derived accurately from the current-pulse experiment because of the difficulty of estimating the effective surface area of the powder-pressed electrode. The $\tilde{D}$ value in sample D obtained by using the BET surface area (22 $m^2 g^{-1}$, Table 1) was 1.8×10^{-14} cm^2 s^{-1} at 20 °C. This value was significantly lower than that using the geometric surface area (5.4×10^{-10} cm^2 s^{-1}). Since the charge and discharge processes do not seem to

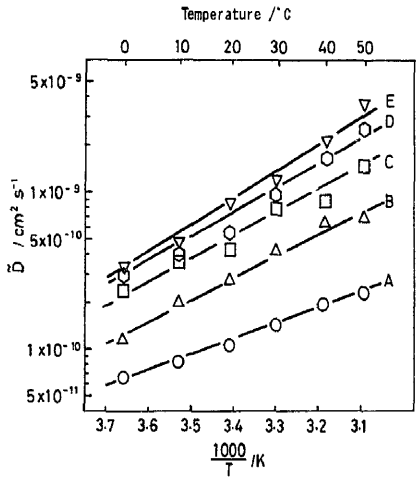

Fig. 8. Temperature dependence of proton diffusion coefficient for samples A to E.

Table 3
D_0 and ΔH values for proton diffusion in nickel hydroxide samples

Sample	D_0 ($cm^2 s^{-1}$)	ΔH (eV)
A	2.78×10^{-7}	0.20
B	1.46×10^{-5}	0.27
C	3.44×10^{-5}	0.28
D	1.31×10^{-4}	0.31
E	4.40×10^{-4}	0.33

change the surface condition, however, the relative values of $\tilde{D}$ in Fig. 8 may reflect actual variations with temperature and sample type.

From the slope of the lines in Fig. 8, the enthalpy (ΔH) and D_0 values for proton diffusion were obtained (Table 3) using the following relationship:

$$\tilde{D} = D_0 \exp(-\Delta H/RT) \quad (4)$$

It is found that the D_0 values increase with an increase in cobalt content. The β-$Ni(OH)_2$ has a brucite-type structure with a hexagonal unit cell and the crystal lattice consists of stacked layers [8]. As reported previously [12], nickel hydroxide with a smaller crystalline size gave higher $\tilde{D}$ and D_0 values. From the data given in Table 3, cobalt addition above 0.65 wt.% causes the FWHM values to be small, and this indicates an increase in the crystalline size of the hydroxides. Moreover, the interlayer distance of the hydroxide diminishes to a small extent as the cobalt content increases, as seen in Fig. 3. In spite of the increase in the crystalline size and diminishment in the interlayer distance, the $\tilde{D}$ and D_0 values increase with increase in cobalt content.

Takehara et al. [17] have measured the ΔH values of nickel hydroxide which not contains cobalt using a potential decay measurement, and have reported $\Delta H = 0.22$ eV [17]. This value is close to those for samples A and B that contain a small amount of cobalt. The observed ΔH values in the 0.20–0.33 eV range are typical of ions diffused in the layered materials [18].

References

[1] I. Matsumoto, M. Ikeyama, T. Iwaki and H. Ogawa, *Denki Kagaku, 54* (1986) 159.
[2] I. Matsumoto, M. Ikeyama, T. Iwaki, Y. Umeo and H. Ogawa, *Denki Kagaku, 54* (1986) 164.
[3] T.A. Edison, *US Patent No. 1 083 356* (1914).
[4] S.U. Falk and A.J. Salkind, *Alkaline Storage Batteries*, Wiley, New York, 1969.
[5] D. Yamashita, *Denki Kaguku, 31* (1963) 228.
[6] D.F. Pickett and J.T. Maloy, *J. Electrochem. Soc., 125* (1978) 1027.
[7] D.H. Fritts, *J. Electrochem. Soc., 129* (1982) 118.
[8] P. Oliva, J. Leonardi, J.F. Laurent, C. Delmas, J.J. Braconnier, M. Figlarz, F. Fievet and A. Guibert, *J. Power Sources, 8* (1982) 229.
[9] M. Oshitani, Y. Sasaki and K. Takashima, *J. Power Sources, 12* (1984) 219.
[10] R.D. Armstrong, G.W.D. Griggs and E.A. Charles, *J. Appl. Electrochem., 18* (1988) 215.
[11] R.D. Armstrong and E.A. Charles, *J. Power Sources, 25* (1989) 89.
[12] K. Watanabe, T. Kikuoka and N. Kumagai, *J. Appl. Electrochem., 25* (1995) 219.
[13] S. Basu and W.L. Worrell, in J.N. Mundy, P.D. Vashita and G.K. Shenoy (eds.), *Fast Ion Transport in Solids*, North-Holland, Amsterdam, 1979, p. 149.
[14] N. Kumagai, S. Tanifuji, T. Fujiwara and K. Tanno, *Electrochim. Acta, 37* (1992) 1039.
[15] P.G. Dickens, S.J. Hibble and R.H. Jarman, *J. Electron. Mater., 10* (1981) 999.
[16] R.D. Shannon, *Acta Crystallogr. A32* (1976) 751.
[17] Z. Takehara, M. Kato and S. Yoshizawa, *Electrochim. Acta, 16* (1971) 833.
[18] N. Kumagai and K. Tanno, *Electrochim. Acta, 36* (1991) 935.